



1 **Comparison of observed borehole temperatures in Antarctica**  
2 **with simulations using a forward model driven by climate model**  
3 **outputs covering the past millennium**

4 Zhiqiang Lyu<sup>1</sup>, Anais J. Orsi<sup>2</sup>, Hugues Goosse<sup>1</sup>

5 <sup>1</sup>Université catholique de Louvain (UCLouvain), Earth and Life Institute (ELI), Georges Lemaître Centre for Earth  
6 and Climate Research (TECLIM), Place Louis Pasteur, B-1348 Louvain-la-Neuve, Belgium

7 <sup>2</sup>Laboratoire des Sciences du Climat et de l'Environnement (IPSL/CEA-CNRS-UVSQ UMR 8212), CEA Saclay,  
8 91191 Gif-sur-Yvette CEDEX, France

9 **Correspondence:** *Zhiqiang Lyu* (*zhiqiang.lyu@student.uclouvain.be*)

10 **Abstract.** The reconstructed surface temperature series from boreholes in Antarctica have significantly contributed to  
11 our understanding of centennial and multi-decadal temperature changes and thus provides us a good way to evaluate  
12 the climate model ability to reproduce low-frequency climate variability. However, up to now, there were no  
13 systematic model-data comparisons based on temperature from boreholes at regional or local scale in Antarctica.  
14 Here, we discuss two different ways to perform such a comparison using boreholes measurements and the  
15 corresponding reconstructions of surface temperature at West Antarctic Ice Sheet (WAIS), Larissa, Mill Island and  
16 Styx in Antarctica. The standard approach is to compare climate model outputs at the grid point closest to each site  
17 with the reconstructions in the time domain derived from the direct borehole temperature observations. Although some  
18 characteristics of the reconstructions, for instance the non-uniform smoothing, limit to some extent the model-data  
19 comparison, several robust features can be evaluated. In addition, a more direct model-data comparison based on the  
20 temperature measured in the boreholes is conducted using a forward model that simulates explicitly the subsurface  
21 temperature profiles when driven with climate model outputs. This comparison in the depth domain provides many  
22 consistent signals with those in the time domain, but also suggest some information that we cannot extract from the  
23 comparison in the time domain. The major results from these comparisons are used to define some metrics derived  
24 from the borehole temperature data for future model-data comparison, and demonstrate the spatial representativity of  
25 the sites chosen for the metrics. The long term cooling trend in West Antarctica from 1000 to 1600 CE (-1.0 °C) is  
26 generally reproduced by the models, but often with a weaker amplitude. The 19th century cooling in the Antarctic  
27 Peninsula (-0.94°C) is not reproduced by any of the models, which tend to show warming instead. The trend over the  
28 last 50 years is generally well reproduced in West Antarctica and at Larissa (Antarctic Peninsula), but overestimated at  
29 other sites. The wide range of simulated trends indicates the importance of internal variability on the observed trends,  
30 and show the value of model-data comparison to investigate the response to forcings.

31



32 *Copyright statement.* This work is distributed under the Creative Commons Attribution 4.0 License.

### 33 **1. Introduction**

34 Although most of the world has been steadily warming over the last few decades, the temperature trend in Antarctica is  
35 not homogeneous (Jones et al., 2016). Several syntheses relying on instrumental air temperatures records have shown  
36 a large recent warming over the AP and parts of West Antarctica, but the trend for the other parts of the Antarctic  
37 continent remains less clear (Chapman and Walsh, 2007; Nicolas and Bromwich, 2014; Steig et al., 2009; Turner et  
38 al., 2005). The sparse instrumental data and the series covering generally less than 60 years do not allow to  
39 characterize well the large interannual to multi-decadal variability at high southern latitudes. The mechanisms at the  
40 origin of recent changes are thus still uncertain (Goosse et al., 2012; Jones et al., 2016; Nicolas and Bromwich, 2014).  
41 Proxy-based reconstructions offer the opportunity to place the recent temperature changes in a longer context. Thanks  
42 to their relatively good spatial coverage and their high resolution, the reconstructions based on water stable isotopes  
43 derived from ice core have provided important information on temperature variability during past two millennia over  
44 Antarctica. They indicate a significant cooling trend during the preindustrial period across all Antarctic regions and  
45 confirm the strong spatial heterogeneity of the recent warming (Goosse, 2012; Schneider et al., 2006; Stenni et al.,  
46 2017). However, the link between the isotope records and local climate is complicated, and this introduces significant  
47 uncertainties in the reconstructions (Stenni et al. 2017, Klein et al., 2019).

48 Borehole temperature observations provide another opportunity to reconstruct surface temperature and several  
49 studies have demonstrated their interest, particularly over Antarctica (i.e. Barrett et al., 2009; Muto et al., 2011; Orsi et  
50 al., 2012; Zagorodnov et al., 2012; Roberts et al., 2013; Yang et al., 2018). Since the variable measured in the borehole  
51 is the temperature itself, i.e. the variable that is reconstructed, no calibration is required against independent  
52 climatologic data such as instrumental data. Nevertheless, the characteristics of heat conduction that blurs the surface  
53 temperature history makes the reconstruction mathematically undetermined. Several approaches have been proposed  
54 to overcome the problem as synthesized in Orsi et al (2012), for instance the Bayesian Reversible Jump Markov chain  
55 Monte Carlo (Dahl-Jensen et al., 1999), the generalized least-squares inversion (Muto et al., 2011; Orsi et al., 2012;  
56 Yang et al., 2018), and the Tikhonov regularization method (Roberts et al., 2013). By applying these methods, the  
57 reconstructed temperature series have presented evidence of the existence of cold conditions corresponding to a Little  
58 Ice Age in West Antarctica from 1300 to 1800 CE (Orsi et al., 2012), as well as of a recent warming trend in West  
59 Antarctica (Barrett et al., 2009; Orsi et al., 2012; Yang et al., 2018), at some high elevation sites of the East Antarctica  
60 (Muto et al., 2011; Roberts et al., 2013) and over the Antarctica Peninsula (Zagorodnov et al., 2012), though the timing  
61 and magnitude vary between regions.

62 The reconstructed temperatures based on isotopic composition have been compared to results of climate models.  
63 Most models display a relatively large and homogenous warming over Antarctica since 1850, which is inconsistent  
64 with the signal inferred from the isotope records (Goosse et al., 2012; Klein et al., 2019; Stenni et al., 2017, Abram et  
65 al. 2016). This disagreement may be due to the uncertainties in the reconstructions, or due to the uncertainties in the  
66 climate models that may overestimate the response to greenhouse gas forcing or underestimate the natural climate  
67 variability in the region (Jones et al., 2016; Neukom et al., 2018). However, a recent study assessing the link between



68 isotope record from ice cores and regional climate over Antarctica using pseudoproxy and data assimilation  
69 experiments has not been able to identify any systematic bias in reconstructions on continental scale temperatures  
70 based on  $\delta^{18}\text{O}$  (Klein et al., 2019).

71 Up to now, there were no systematic model-data comparison for temperature reconstructed from boreholes at  
72 regional or local scale in Antarctica. This is, on the one hand, due to the characteristics of the inversion that imposes  
73 smoothing on a time window that increases as we go back in time and makes the comparison with the simulated  
74 surface temperature difficult (Beltrami et al., 2006; Harris and Gosnold, 1999). Additionally, some reconstructions  
75 have an uncertainty range of the same magnitude as the full variability provided by the climate model results, which  
76 seriously limits the interest of data-model comparison.

77 As some of the difficulties in the comparison between the simulated surface temperature and the ones reconstructed  
78 from borehole come from the inversion procedure, comparing directly the observed profile with the one obtained  
79 using a one-dimensional heat advection and diffusion forward model driven with climate model can provide new  
80 insight. This approach is an example of the application of Proxy System Models (PSM) that reproduce directly  
81 processes responsible for the signal recorded in the archive (Evans et al., 2013). PSMs have been applied recently for  
82 several proxies, such as tree ring width (Evans et al., 2013) or water-isotope in ice cores, corals, tree ring cellulose, and  
83 speleothem calcite (Dee et al., 2014). The use of climate model outputs to drive a borehole temperature forward model  
84 has demonstrated the strong coupling between near-surface air and ground temperature changes over decades to  
85 centuries (e.g. Beltrami et al., 2005; García-García et al., 2016; González-Rouco et al., 2003, 2006), and validated  
86 climate model outputs (e.g. Beltrami et al., 2006; Stevens et al., 2008).

87 Nevertheless, using a PSM also introduces some uncertainties that must be taken into account. A critical point for  
88 borehole temperature is the potential influence of long-term climate changes, such as glacial to inter-glacial cycles,  
89 that is difficult to estimate (Orsi et al., 2012, Rath et al., 2012). In addition, the simulated subsurface temperature  
90 profiles are sensitive to model parameters and inputs, such as snow accumulation, ice thickness, geothermal heat flow  
91 and the physical properties of ice or ground, which may have significant uncertainties.

92 Previous studies using forward models driven by climate model outputs were focused on ground temperature and  
93 not to borehole obtained in the ice. Here, we will fill this gap by simulating directly subsurface temperature for the  
94 publicly available borehole profiles covering the past centuries in Antarctica, using the one-dimensional heat  
95 advection and diffusion forward model of Orsi et al.(2012). Our goal here is to provide a protocol for evaluating the  
96 climate model ability to reproduce observed low-frequency (multi-decadal to centennial scale) variability. We will  
97 analyze two model-data comparison methods to identify the potential advantage and drawbacks of each approach. The  
98 easiest way is in to directly compare the surface temperature reconstructed from the borehole measurements with the  
99 surface temperature time series simulated by the climate model at the grid point closest to each site. The second way is  
100 to compare the simulated subsurface borehole temperature with the measurement by driving the forward model with  
101 climate model outputs. In this case, we analyze the temperature at a fixed time (the one when observation where taken)  
102 as a function of depth. For simplicity, we will later refer to those two methods as a comparison in the time domain and  
103 depth domain, respectively.



104 This study is organized as follows. The borehole temperature observations, the climate model results, the forward  
105 model and the sensitivity of the results to key parameters of the forward model are briefly described in Section 2.  
106 Section 3 presents the comparison of simulated and reconstructed surface air temperatures, and the comparisons of  
107 simulated and observed subsurface temperature profiles. Some metrics of Antarctic climate for model validation are  
108 proposed and discussed in Section 4. Conclusions are given in Section 5.

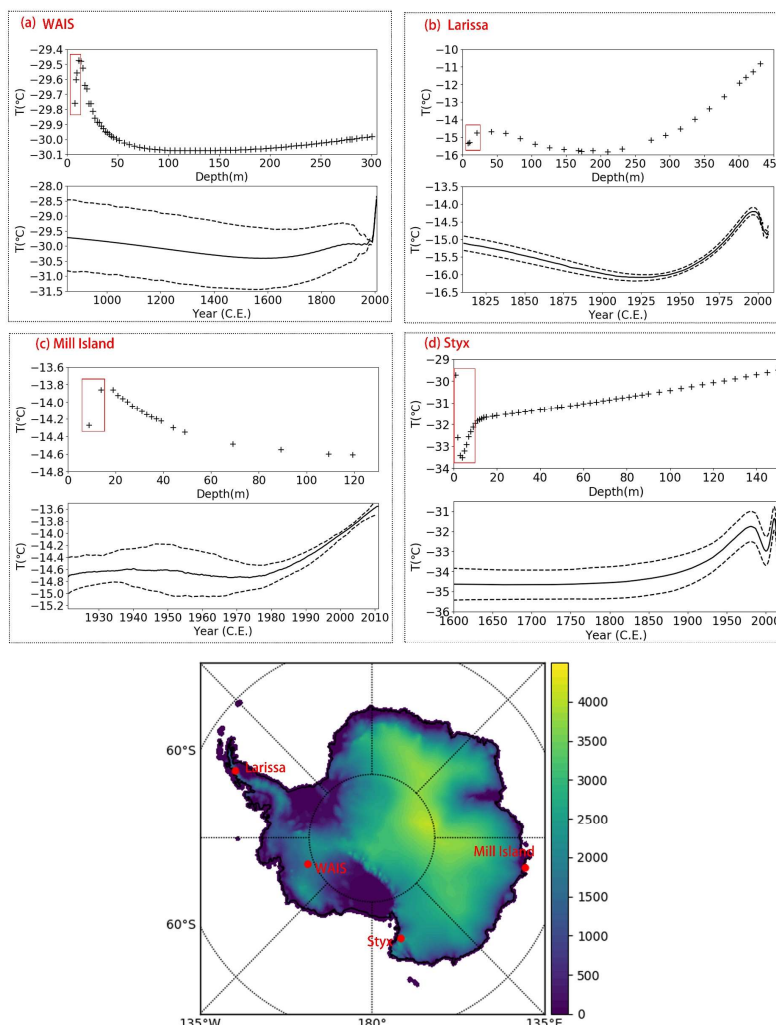
## 109 2. Data and Methods

### 110 2.1 Borehole temperature observations and reconstructed surface temperature

111 The data used in this study includes measured temperature in four boreholes in Antarctica. We refer to them as  
112 ‘WAIS’, ‘Larissa’, ‘Mill Island’, and ‘Styx’ respectively. Figure 1 and Table 1 provide their locations and  
113 corresponding references. The borehole temperature profiles were sampled in January 2008 and January 2009  
114 (WAIS), December-February 2009/10 (Larissa), the summer of 2009/10 (Mill Island), and the summer of 2014/15  
115 (Styx). As shown in Fig. 1 (in red rectangles), the borehole temperatures are affected by the seasonal cycle in the upper  
116 15 meters (Bodri, et al., 2011, Chap. 1), which is not adequate for the reconstruction of annual mean surface  
117 temperature. Consequently, only the depth under 15 meters is used to reconstruct the surface temperature history and  
118 to compare with simulated subsurface temperature profiles.

119 **Table 1.** Location of the four boreholes. Elevation is in meters above sea level (m a.s.l.)

Region	Referenced Name	Latitude	Longitude	Elevation (m a.s.l)	Reference
West Antarctica	WAIS	79°28'S	112°05'W	1766	Orsi et al., 2012
Antarctic Peninsula	Larissa	66°02'S	64°04'W	1975.5	Zagorodnov et al., 2012
East Antarctic	Mill Island	65°33'25.84"S	100°47'11.44"E	503	Roberts et al., 2013
Western Coast of the Ross Sea	Styx	73°51.10'S	163°41.22"E	1623	Yang et al., 2018



120  
 121 **Figure 1.** Observed Borehole profiles, corresponding reconstructed surface temperature and the location at four sites in Antarctica.  
 122 The symbols (+) show the measured borehole temperature. The dashed lines represent the reconstructed uncertainty and the thick  
 123 black line is the mean reconstructed temperature. In (a), (b), (c), and (d), the red rectangles represent the borehole temperatures that  
 124 are influenced by the seasonal cycle. The bottom panel shows the location of these four boreholes and their corresponding elevation  
 125 over Antarctica.

126 The temperature reconstructions and uncertainty estimates for the four boreholes are shown on Fig. 1. For WAIS,  
 127 Styx, and Mill island, the reconstructed surface temperature series (Fig. 1 a, c, d) are computed using a generalized  
 128 least-squares algorithm (e.g. Orsi et al., 2012). For Larissa, the surface temperature is recovered by the Tikhonov  
 129 regularization algorithm (Zagorodnov et al., 2012). This method has been proved to be valid for inverse problems such  
 130 as the reconstructions based on borehole temperature observations, and the details of this method are explained in  
 131 (Nagornov et al., 2001, 2006).



## 132 2.2 Climate model simulations

133 The surface air temperature used in this study is extracted from PMIP3-CMIP5 experiments (Braconnot et al., 2012,  
134 <http://pmip3.lscce.ipsl.fr/>; Taylor et al., 2012, <http://cmip-pcmdi.llnl.gov/cmip5/>). Table 2 shows the characteristics  
135 and the corresponding references. These simulations both cover the past 1000 (850-1850 AD) and the historical period  
136 (1850-2005 AD). CESM1-CAM5 and MPI-ESM-P are not continuous in 1850. Such discontinuity for the variables  
137 employed in 1850 falls within the range of variability of the simulated climate, thus merging it with the historical  
138 period have limited effect on the results (Klein et al. 2016). These simulations are driven by natural (orbital, solar  
139 irradiance, volcanic) and the anthropogenic (well-mixed greenhouse gases, ozone, aerosols, land use/land cover)  
140 forcings (Schmidt et al., 2011, 2012). Note that, BCC-CSM1-1 and IPSL-CM5A-LR ignore the impact of land  
141 use/land cover, and IPSL-CM5A-LR does not consider any variations in aerosols and tropospheric ozone. Further  
142 description of the simulations and the forcing can be found for instance in Klein et al., (2016). For CESM1, an  
143 ensemble of simulations is available, providing an estimate of the internal variability as simulated by this model.

144 **Table 2** Climate model simulations used to drive the forward model

Name	Model resolution (lat × lon)	Number of simulations for 850-1850 period	Number of simulations for 1850-2005 period	Reference
CESM1-CAM5	96 × 144	12	12	Otto-Bliesner et al., (2016)
GISS-E2-R	90 × 144	1	1	Schmidt et al., (2014)
IPSL-CM5A-LR	96 × 96	1	1	Dufresne et al. (2013)
MPI-ESM-P	96 × 192	1	1	Stevens et al., (2013)
CCSM4	192 × 288	1	1	Gent et al. (2011)
BCC-CSM1-1	64 × 128	1	1	Wu et al., (2014)

## 145 2.3 The Forward Model Description

146 The forward model used herein to simulate the propagation of the signal coming from the surface temperature history  
147 into the subsurface is based on the one-dimensional heat and ice flow equation (Alley and Koci, 1990):

$$148 \quad \rho c_p \frac{\partial T}{\partial t} = \frac{\partial}{\partial z} \left( k \frac{\partial T}{\partial z} \right) - \rho c_p w \frac{\partial T}{\partial t} + Q \quad (1)$$

149 where  $T$  is the temperature,  $t$  is the time,  $c_p$  is the heat capacity,  $\rho$  is the density of firn/ice,  $z$  is the depth,  $w$  is the  
150 downward velocity of the firn/ice,  $Q$  is the heat production term. The term on the left side represents the change in  
151 heat content and the right terms are the rate of temperature change due to conduction, advection and heat production,  
152 respectively. Important model parameters are summarized in Table 3.

153



154 **Table 3** Optimal parameters used to simulate subsurface temperature profile in the forward model driven by the reconstruction for  
155 each site: (a) WAIS; (b) Larissa; (c) Mill Island; (d) Styx

Site	Surface temperature for steady state (°C)	Accumulation rate (m/second)	Temperature (T) at bottom (°C)	T gradient at bottom (°C/m)	Ice thickness (m)
WAIS	-29.73	$6.97 \times 10^{-9}$	-4.685	0.0256	3400
Larissa	-16	$4.147 \times 10^{-8}$	-10.2	-0.04	447.73
Mill Island	-14.6	$4.53 \times 10^{-8}$	-14.6	0	500
Styx	-32.5	$2.6985 \times 10^{-9}$	-20.5	0.022	550

156 In the model, the density profile, ice thickness and accumulation rates are derived from onsite measurements  
157 according to the descriptions in the original studies while some parameters, such as heat capacity  $c_p$ , thermal  
158 diffusivity  $k$  and heating term  $Q$ , are obtained using classical formulations (Cuffey and Paterson, 2010, Chap. 9). The  
159 basal temperature and heat flux for WAIS, Larissa, and Styx are determined using the lower “undisturbed” sections of  
160 the measured borehole temperature extrapolated to the bottom, and for Mill Island, the heat flux is set to zero,  
161 following the original publication. The vertical discretization of the model is not homogenous. For WAIS, a vertical  
162 step of 1 m for the upper 500 m and up to 25 m for the deepest part, and for other sites where the depth of borehole is  
163 close or less than 500 m, the step is set to 1 m for overall depth.

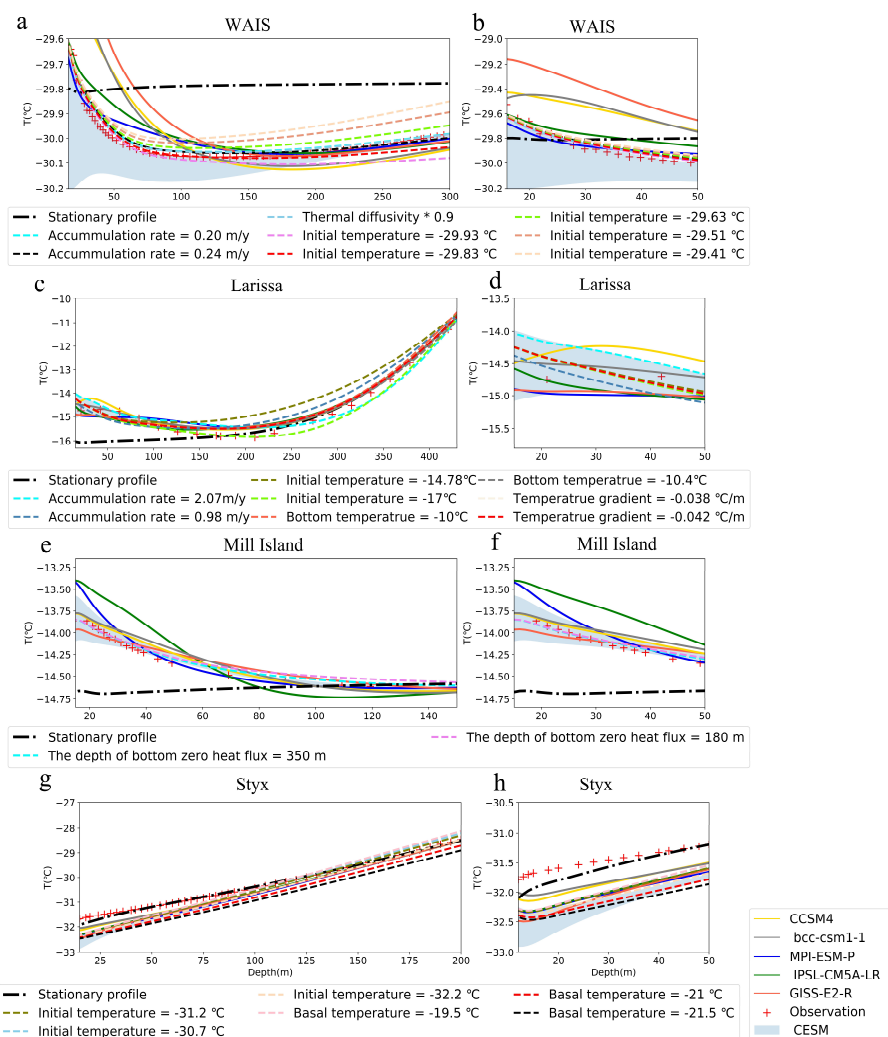
164 Before the forward model is driven by the climate model results, it is initialized with a stationary profile, which is  
165 generated after a 20000-year model run with a constant climate history and a realistic seasonal cycle. The mean  
166 surface temperature is set to the recent annual average temperature and the season cycle is determined by simplifying  
167 the average over weather station data following Eq. 2 (Orsi et al., 2012).

168 
$$T(t) = 10(\cos(2\pi t) + 0.3 \cos(4\pi t)) \quad (2)$$

169



170 **2.4 Sensitivity of subsurface temperature to model parameters**



171  
 172 **Figure 2.** Comparison of borehole temperature profiles outputs of 1) GCMs surface temperature time series with optimal  
 173 parameters (solid lines), and 2) sensitivity tests using the temperature history of once CESM member (dashed lines) at each site. (a)  
 174 WAIS: 15-300m; (b) WAIS: 15-50m; (c) Larissa: 15-430 m; (d) Larissa:15-50m; (e) Mill Island:15-150m; (f) Mill Island:15-50m;  
 175 (g) Styx:15-200m; (h) Styx:15-50m. The shade area represents the simulated subsurface temperature ensemble driven by CESM  
 176 using optimal parameters. The thick dash-dot line denotes the stationary profile at each site.

177 In order to assess the uncertainty in the model-data comparison related to the parameters of the forward model, it is  
 178 necessary to perform a series of sensitivity experiments as shown on Fig. 2. We made different tests for the key  
 179 parameters using the values proposed in the original publications (Table 1) and following the protocol of Orsi et al.  
 180 (2012).





181 The range of tested model parameters in the forward model can influence significantly the shape of simulated  
182 subsurface temperature (Fig. 2), which is in good agreement with the previous studies at those sites.

183 At WAIS-Divide, the spread of the sensitivity tests is lower than the spread if the different scenarios. An increase in  
184 the accumulation rate will reduce the temperature gradient in the borehole profile, but the effect is much weaker than  
185 the difference in temperature histories from the different models. A change in the initial temperature used to calculate  
186 a the starting steady state profile has an influence on the slope of the profile in the deeper part and depth of the  
187 temperature minimum, contributing to the uncertainty in the intensity of the pre-1900 cooling trend and the timing of  
188 the temperature minimum.

189 At Larissa, the effect of the bottom boundary conditions is important in setting up the temperature gradient from the  
190 bottom to 300 m, and therefore, we will not interpret that segment of the data in terms of climate. It is also evident in  
191 Fig. 2c that the different temperature histories produce a very similar depth profile over that interval.

192 At Mill island, although the borehole profile is shallow, the ice thickness is much deeper, but unknown. Here we  
193 modeled this by assuming a zero heat flux bottom boundary at various depth. This sensitivity is weak over the data  
194 interval, and the borehole profile is dominated by the surface temperature history.

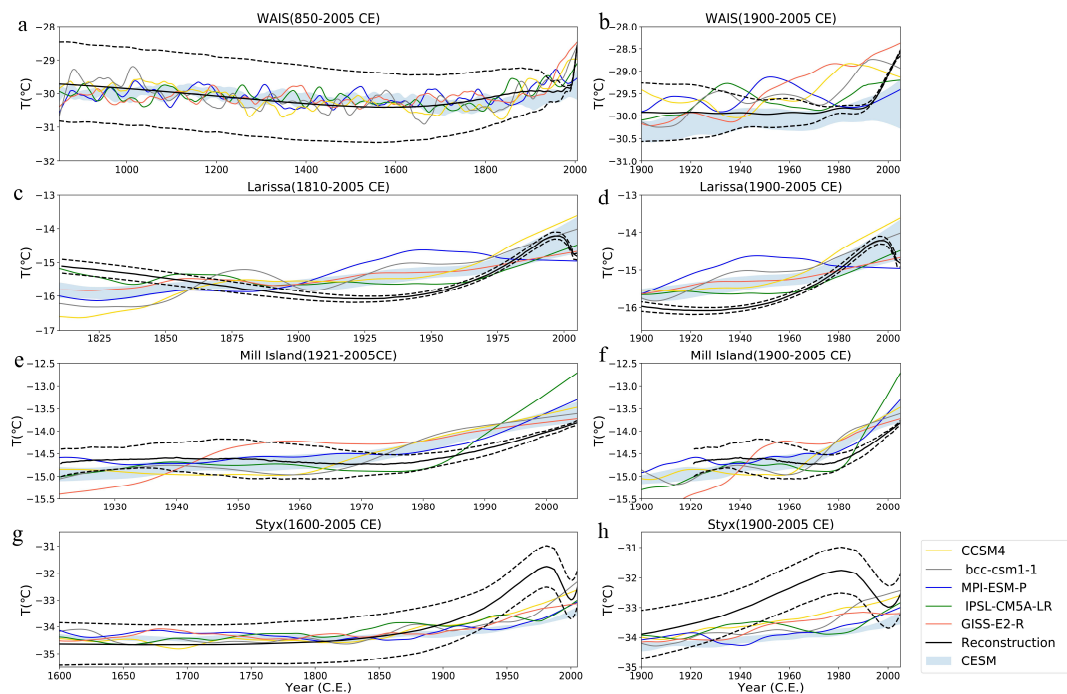
195 At Styx, the boundary conditions are adjusted to reproduce the slope of the temperature profile in the deeper part  
196 (100-200m), but the deviation in the top 100 m show that there is climate information stored in the upper part of the  
197 profile, and that this profile cannot be fully determined by boundary conditions.

198 This confirms that the internal climate variability and different characteristics of these climate models are the  
199 dominant source of the differences and that the model-data comparison provides a robust evaluation of simulated  
200 temperature time series. For the deeper part of WAIS and Larissa, as the shape of subsurface temperature profiles is  
201 influenced by the parameters of the forward model, the evaluation of the long-term cooling trend is more uncertain.



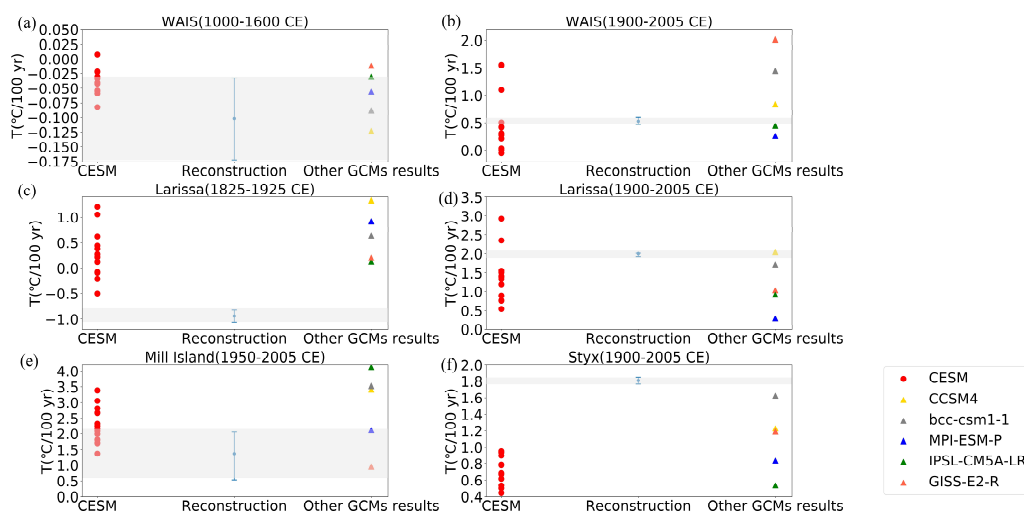
202 3. Results

203 3.1 Comparison between the simulated temperature and reconstructions



204

205 **Figure 3.** Comparison between reconstructed surface temperature series from borehole and the climate model outputs at the  
206 grid-point closest to each borehole site. The borehole reconstructions are in black and their uncertainty ranges given by the dashed  
207 lines. Color lines correspond to the climate model results. The shaded area represents the mean  $\pm 1$  standard deviation of CSM  
208 model ensemble. For the left column, a 50-year Lowess smoothing has been applied for the WAIS and Styx time series; Larissa and  
209 Mill Island are smoothed using 10-year and 3-year windows respectively. The time series in the right column is smoothed using  
210 3-year from 1900 to 2005 C.E.



211

212 **Figure 4.** Linear trends for the four boreholes over different period: (a) WAIS: 1000 to 1600 C.E.; (b) WAIS: 1900 to 2005 C.E.; (c)  
213 Larissa:1825 to 1925 C.E.; (d) Larissa:1900 to 2005 C.E. (e) Mill Island: 1950 to 2005 C.E.; (f) Styx:1900 to 2005 C.E..

214 Figure 3 displays the comparisons between climate model results and temperature reconstructions from borehole for  
215 the four selected sites. In order to remove the bias on the mean state for each climate model, anomalies are shown  
216 using the total period covered by each reconstruction as reference. Due to the nature of physical diffusion, the heat  
217 propagation acts similarly as a low-pass filter. The reconstructions thus suffer from an attenuation of high frequency  
218 temperature variability that becomes stronger as times goes back (Beltrami et al., 2006; Harris and Gosnold, 1999).  
219 For instance, in the reconstructed surface temperature of Styx, the point corresponding to 1800 CE in the curve may  
220 represent an average temperature between around 1600 CE and 1900 CE while at 1900 CE it corresponds to an  
221 average over around 200 years. This characteristic complicates the model-data comparison and trends as shown on  
222 Fig. 3 must be interpreted carefully because of this inhomogeneous smoothing.

223 Because of the internal variability of the system, a single simulation is not expected to reproduce well all the  
224 characteristics of the observed variations. The difference can be large, in particular at the local level (e.g. Goosse et al.  
225 2005) but the observations should correspond to a credible member of an ensemble of simulations. Ensuring this  
226 compatibility can be achieved using various techniques but the first step is to simply check if the reconstruction is  
227 within the range provided by the ensemble (e.g. PAGES2k-PMIP 2015).

228 Considering the large uncertainty range in these reconstructions, the climate models are visually able to reproduce  
229 the general characteristics of reconstructed temperature variability, particularly in the long-term cooling during the  
230 last millennium and the recent warming (Fig. 3 and 4). Nevertheless, disagreements have also been identified.

231 The first major feature in the data is the long-term cooling trend, visible at the WAIS-Divide and Larissa sites. At  
232 Larissa (Antarctic Peninsula), the borehole temperature reconstruction finds a cooling trend of  $-0.94 \pm 0.12$  °C/century  
233 from 1825 to 1925 (Zagorodnov et al., 2012). None of the models are able to reproduce this observation, and instead,  
234 they all show a warming trend of comparable magnitude (Fig. 3c and 4c). At WAIS-Divide, the borehole temperature  
235 inversion also shows a long-term cooling trend, from 1000 to about 1600 C.E., with a magnitude of  $-0.10 \pm$



236 0.07°C/century (Fig. 3a). The large uncertainty in the long term trend is principally due to the uncertainty in the initial  
237 surface temperature (Fig. 2a; Orsi et al., 2012, their Fig. 3). The quantitative comparison between the trend of  
238 reconstructions and climate model outputs (Fig. 4a) indicates that the simulations generally show a cooling trend over  
239 1000-1600 CE, in agreement with previous studies (e.g., Goosse et al. 2012, Abram et al. 2016, Klein et al. 2019), but  
240 with a lower amplitude, particularly GISS (-0.01°C/century) and IPSL (-0.03°C/century), but most remain within the  
241 lower end of the reconstructed uncertainty range. This long-term cooling trend is a feature of the Antarctic climate that  
242 is visible in many other ice core records (Stenni et al., 2017). A recent compilation of 2K datasets calculated a trend of  
243 -0.26 to -0.4°C/1000 years for the period 0-1900 AD for the Antarctic continental average (Stenni et al., 2017). In the  
244 high latitudes of the Southern Hemisphere, the origin to this millennial-scale cooling is currently not well understood,  
245 but an intermediate complexity model has shown a multi-millennial cooling in summer because of a delayed response  
246 to the decrease in local spring insolation (Renssen et al., 2005) with also a potential influence of volcanic forcing  
247 (Goosse et al. 2012, Abram et al. 2016, Stenni et al. 2017).

248 A second feature of the data is a warming trend in the twentieth century, which started at different times in the  
249 different records. Styx shows an early warming trend from 1900 to 1980, and a stabilization of the temperature  
250 afterwards (Fig. 3h). Models tend to show the opposite timing, with nearly no trend from 1900 to 1960, and a late  
251 warming trend that differs in amplitude between models. Overall, the warming of the 20th century is about half of  
252 what is observed (Fig. 4f), with bcc (1.63°C/century) and CCSM4 (1.23°C/century) having the largest trends, closest  
253 to the observations (1.81°C/ century).

254 Larissa shows a temperature minimum in 1940's, followed by a steady warming trend until around 1995. The  
255 magnitude of the 20th century trend is 1.99°C/century. Most model reproduce the timing of the warming reasonably  
256 well, with the exception of MPI, which shows an early warming, but no trend in 1940-2005, and GISS, which has a  
257 very muted trend. If the trend present in the other models is too low, it is rather because of the lack of cooling in the  
258 preceding century, than because of errors in the latest decades.

259 Mill Island shows a late warming trend starting in the 1980's. Models tend to overestimate this trend (Fig. 4e), in  
260 particular IPSL, bcc and CCSM4. Similarly to Mill Island, WAIS-Divide also shows a positive trend over the period  
261 1900-present that intensifies after 1980. The amplitude of the 20th century warming (0.53 °C/century) is well  
262 simulated, but the start of the trend is often too early, with the exception of CESM, bcc and IPSL, which show a late  
263 warming trend (Fig. 3b).

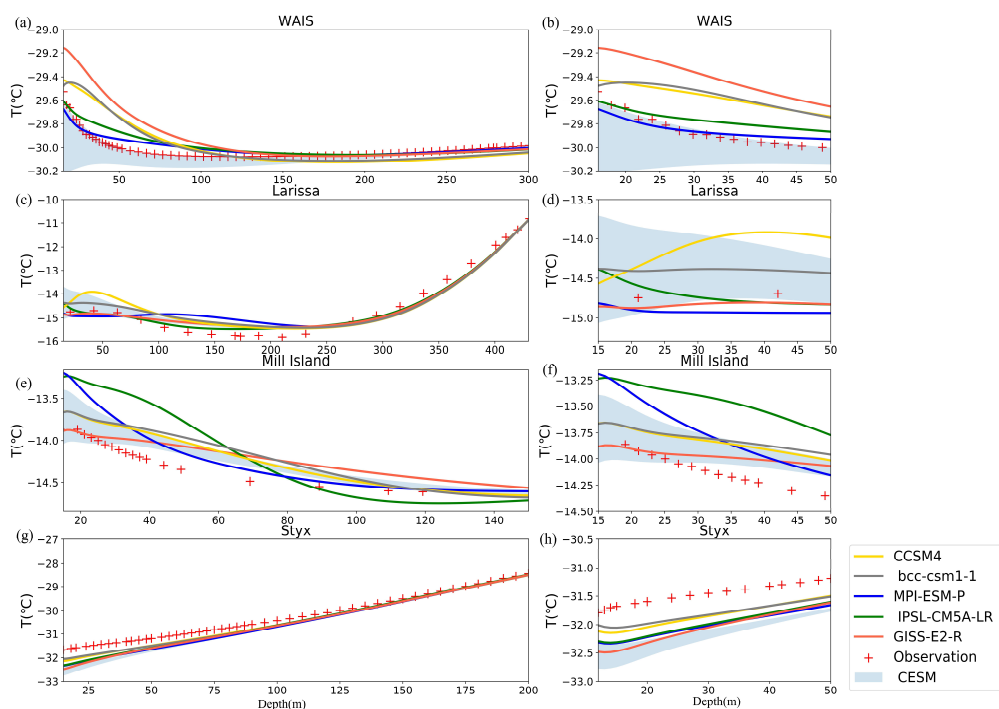
264 Overall, the large variability of the trends over the 20th century within the CESM ensemble for WAIS and Larissa  
265 suggests that many apparent model disagreements for those sites can be due to internal variability while the  
266 disagreement may be more profound for Styx and Mill Island.

267 However, as stated above, borehole temperature reconstructions are “underdetermined”, which means that there are  
268 many possible temperature histories that can fit the data. The next step is to determine if the differences between  
269 simulated and reconstructed time series can be discriminated when analyzing observed and simulated temperature  
270 profile



### 271 3.2 Comparison of the simulated subsurface temperature with observation

272 The simulated subsurface temperature profile is the results of the superposition of two components: (1) the initial  
273 temperature profile that incorporates the effects of basal heat flux, vertical advection due to ice accumulation and  
274 initial temperature; (2) the subsurface temperature deviations arising from the surface temperature variability. Since  
275 the initial temperature profile for each borehole is obtained by driving the forward model with the optimal parameters  
276 obtained from the original publications describing the reconstructions (see Section 2.4), the differences among the  
277 simulated borehole profiles for each location are caused only by the changes in the upper boundary, i.e. in the climate  
278 model outputs. The simulated subsurface temperature profiles for each borehole are displayed in Fig. 5.



279  
280 **Figure 5.** Comparisons between simulated subsurface temperature and measurements for : (a) WAIS: 15-300 m; (b) WAIS: 15-50  
281 m; (c) Larissa: 15-430 m; (d) Larissa:15-50 m; (e) Mill Island:15-150 m; (f) Mill Island:15-50 m; (g) Styx:15-200 m; (h)  
282 Styx:15-50 m. The shaded area represents the simulated subsurface temperature ensemble driven by CESM ensemble. The right  
283 panel is a zoom over the upper 50 m for each borehole.

284 As previous studies shown (Bodri, Louise, and Vladimir Cermak, 2011, Chap. 2), a ‘U’ shape subsurface  
285 temperature profile is a direct evidence for the past climate change with a minimum that separates the deeper warming  
286 trend due to geothermal heating and shallower warming trend related to a recent temperature increase (Orsi et al.,  
287 2012; Stevens et al., 2008). Among these four sites, WAIS and Larissa have such characteristics of ‘U’ shape curve.  
288 For Mill Island, this is less clear but a significant breaking point in each simulated subsurface temperature profile  
289 reflects the surface temperature warming over recent decades while for Styx such break does not seem to be present at  
290 all, but the slope does increase with depth.



291 Aided by these key properties, we can identify a link between the interpretation in the depth domain and in the time  
292 domain. The analysis of the simulated and observed temperature profile confirm the main conclusion obtained in  
293 section 3.1, in particular with an agreement between model and data on the general tendencies, characterized by a  
294 long-term cooling trend over last millennium and the recent warming. For the deeper part of the profile, the  
295 temperature simulated in experiments driven by MPI, IPSL, GISS at WAIS almost coincides with the corresponding  
296 observations, but they fail to reproduce the depth of the temperature minimum around 120 m in the data. This is  
297 consistent with the fact that IPSL and MPI are at the edge of the reconstructed cooling trend of the last millennium and  
298 GISS present a significant underestimate (Fig. 4a). On the other hand, the CESM ensemble follows the borehole  
299 temperature profile (shaded area on Fig. 5a), and could also reproduce the magnitude of the cooling trend for some of  
300 the members (Fig. 4a). Specifically, the minima in the simulated profiles driven by MPI, IPSL, GISS and CESM  
301 shows the value of  $-30.06$  °C,  $-30.06$  °C,  $-30.07$  °C and a range of  $-30.8$  °C to  $-30.17$  °C respectively, which is very  
302 close to the minimum of  $-30.08$  °C in the observations. At Larissa, the bottom (270-450 m) of the profile is controlled  
303 by boundary conditions (Fig. 2c), and contains no climate information, as demonstrated by the fact that all curves are  
304 on top of each other on Fig. 5c. Additionally, no simulation has a pronounced inflection point around the 170 m as in  
305 the observation. These characteristics are perfectly consistent with the lack of a cooling trend from mid-19th century  
306 to the early 20th century in the simulations (Fig. 3c). We conclude from this that the cooling trend of 1825-1925 is a  
307 robust feature in the data that can be used to benchmark climate models.

308 For the recent warming, we see some significant discrepancies among the simulated subsurface temperatures driven  
309 by different climate models at the four boreholes in the depth domain that are consistent with the signal analyzed in the  
310 time domain. For WAIS, in the uppermost part, the simulated subsurface temperature profiles driven by GISS, CCSM  
311 and bcc display significantly higher temperatures than in the observations, while IPSL and MPI-simulated profiles are  
312 close to the measurements (Fig. 5b). This is in perfect agreement with the too high temperatures in models compared  
313 to the reconstructions in the second half of the 20th century (Fig. 3b). For Larissa, all simulated profiles display an  
314 increasing temperature toward the surface as in observations but with different magnitude and shape (Fig. 5c). The  
315 temperature in the simulation driven by the MPI displays a relatively rapid increase until around 100 m and then is  
316 constant, which is consistent with the near constant temperature from 1940-2005 (Fig. 3d). For the ones driven by  
317 CCSM and bcc, they are warmer than the observations between the depth 15m to 50m, which reflects the consistently  
318 warmer temperature shown in Fig. 3d. IPSL-simulated subsurface temperature profile displays the largest similarity to  
319 the observations, whilst the simulations performed with CESM can cover almost all the observation in the shallow  
320 zone. For Mill Island, the simulated subsurface temperature profiles are warmer than observations above 50 m,  
321 confirming the too large warming trend deduced from the analysis of surface temperature. In particular, the IPSL  
322 model has the largest warming trend (Fig. 3 e, f) and also has the warmest temperature profile (Fig. 5 e, f), followed by  
323 MPI. The borehole data thus is providing constraints to evaluate the different simulations. For Styx, the main  
324 discrepancies occur over the shallow depths, between of 15 m to 60 m, where all the simulations depict colder  
325 condition compared with observations (Fig. 5 g, h), as for the surface temperature over the recent decades on Fig. 3.  
326 Nevertheless, we also find in the depth domain some signals that are not obvious in the time domain. In particular, for  
327 WAIS, one of the CESM runs matches the warming trend of the top 100 m, while in time domain the CESM ensemble



328 was significantly colder than reconstruction over recent decades. The CESM outputs generally follow the data in the  
329 deeper part of the profile (200-300 m), and have an even steeper slope between 100 and 200 m (Fig. 5), while in the  
330 time domain, the cooling trend was underestimated (Fig. 4a). In addition, for WAIS, the simulated subsurface  
331 temperature driven by CCSM4 and bcc over the deeper part of the profile are colder than observations, but start the  
332 warming trend deeper, at about 200 m against 120 m in the observations. This seems puzzling because, in the time  
333 domain, the cooling trend continues until 1800 for CCSM4 (Fig. 2a, yellow), but the larger warming in the last 100  
334 years, is probably shifting the temperature minimum downwards. This example shows that it is difficult to pinpoint the  
335 date corresponding to a temperature minimum in the depth profile, because it depends on the respective speed of  
336 warming and cooling before and after. At Mill Island, in the deeper part (around from 140 m to 100 m) of the profile,  
337 the simulated subsurface temperature profile driven by IPSL, with a slightly decreasing temperature and a colder  
338 climate than observations, is very different from the other ones. However, in the time domain, the difference compared  
339 to other time series for IPSL was much less clear but the consistency between these two domains still exists, and  
340 especially the temperature minimum in 1980 might correspond to the deeper part in the depth domain.

341 The comparison between the analyses in the two domains appears thus complementary and instructive as it  
342 illustrates that the interpretation may be easier in one case or the other. It also shows that the different model runs  
343 produce different borehole temperature profile, and that the observations can help evaluate the models. In particular,  
344 the analysis of the simulated temperature profile confirms that CESM ensemble can reproduce the multi-decadal and  
345 centennial climate variability at WAIS.

#### 346 **4. Proposed metric of Antarctic climate for model validation**

347 In this section, we use the results of the previous section to describe a few metrics that can be used easily to evaluate  
348 the next generation of climate model simulations (e.g. PMIP4-CMIP6, Jungclaus et al., 2017), and investigate the  
349 spatial representativity of the records.

##### 350 **4.1 Metric 1 : last millennium cooling at WAIS Divide**

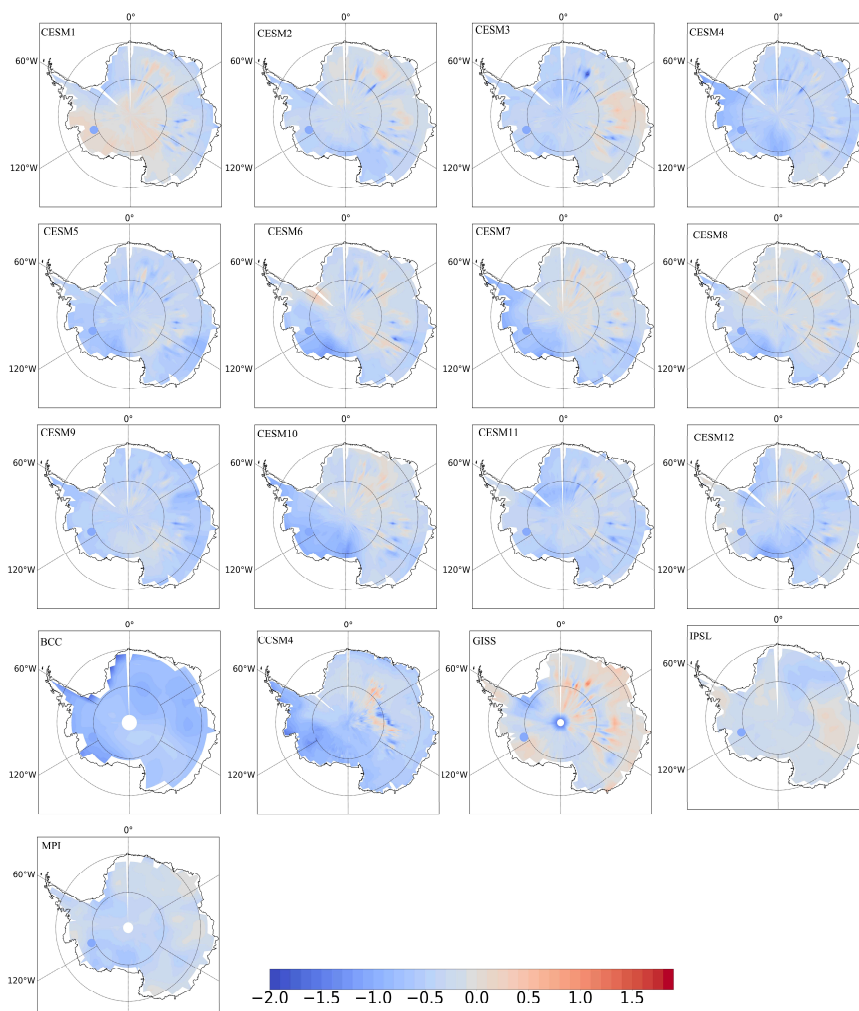
351 Of the four records presented here, WAIS-Divide has the longest retrievable history. We propose here to use the  
352 temperature trend of the period of 1000 to 1600 C.E. as a metric, with the magnitude of  $-0.102 \pm 0.07$  °C/century (Fig.  
353 4a). The end of the cooling trend is not clearly defined by the data, due to the complex time-varying smoothing of the  
354 borehole temperature record, but 1600 C.E. seems to be safely in the cold interval (See Orsi et al., 2012, Fig. 4a for  
355 details). The start of the period is more open, and we chose 1000 C.E. to be compatible with last millennium  
356 simulations. External evidence from a compilation of water isotope records indicates that the cooling trend extended  
357 likely from 0 to 1900 C.E. in many parts of Antarctica (Stenni et al., 2017). It is a robust feature of the Antarctic  
358 climate of the last 2ka, and the WAIS-Divide record is unique in providing a clear quantification of the temperature  
359 trend.

360 In Fig. 6, we show the 1000 to 1600 C.E. surface temperature trend at WAIS-Divide and at other sites in Antarctica  
361 from the models output. Visually, for most simulations, the cooling at the grid point of WAIS-Divide is similar to the  
362 one obtained at many location in West Antarctica. Only the first member of CESM shows a small warming trend in



363 West Antarctica. The large spatial coherence of the trend indicates that, although we are making a single point  
364 comparison, it represents a signal common to a large part of the continent. It is also important to estimate the  
365 magnitude of the trend at WAIS compared to other regions. To do so, we calculate the ratio of the trend of surface  
366 temperature from 1000 to 1600 C.E. at any location with the one at WAIS-Divide (Fig. 7). Except the first member of  
367 CESM, if the value is greater than 1 (shown in red tones), it means the trend at the grid-point is larger than that at  
368 WAIS-Divide; if the value lies between 0 and 1 (shown in blue tones), it means the trend at the grid is less than that  
369 observed at WAIS-Divide. Negative values (i.e., a trend of a different sign compared to WAIS) are not shown and the  
370 corresponding region left blank. Since the goal of Fig. 7 is to show the intensity of cooling at WAIS compared with  
371 other points in Antarctica, the first member of CESM 1, which shows a warming trend close to zero at WAIS, is not  
372 very meaningful but it is still included for completeness. For most of the models, WAIS displays a larger cooling from  
373 1000 to 1600 C.E. than other locations in Antarctica (shown in blue) but with magnitude similar to other grid points in  
374 West Antarctica, which is consistent with the reconstruction of Stenni et al. (2017) that shows the largest cooling in  
375 this region over the period 0-1900 CE C.E (Stenni et al., 2017). The spatial patterns of the trends (Fig. 7) are different  
376 between models, but also within the CESM ensembles, showing that the changes in Antarctica are strongly influenced  
377 by internal variability, even at century timescale. Future work including more sites, or using water isotopes and the  
378 Antarctica-2K database will help constrain the spatial pattern of this trend.  
379





380

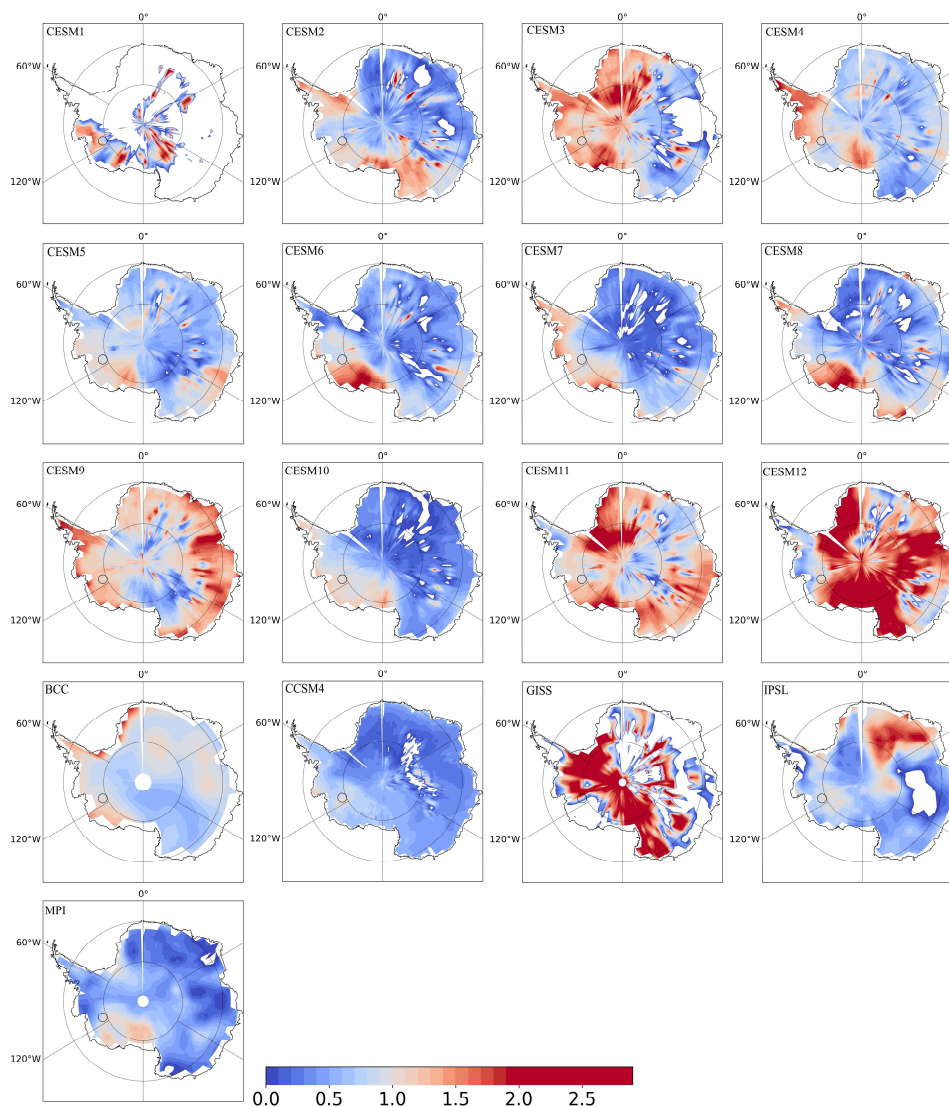
381 **Figure 6.** The simulated (blue-red shading area) and observed (circle) surface temperature trend from 1000 to 1600 C.E. in

382 Antarctica.

383



384



385

386 **Figure 7.** The ratio of the surface temperature trend (blue-red shading area) from 1000 to 1600 C.E between other grids in  
387 Antarctica and WAIS-Divide. The black circle denotes the location of the WAIS Divide.

#### 388 **4.2 Metric 2: nineteenth century cooling at Larissa**

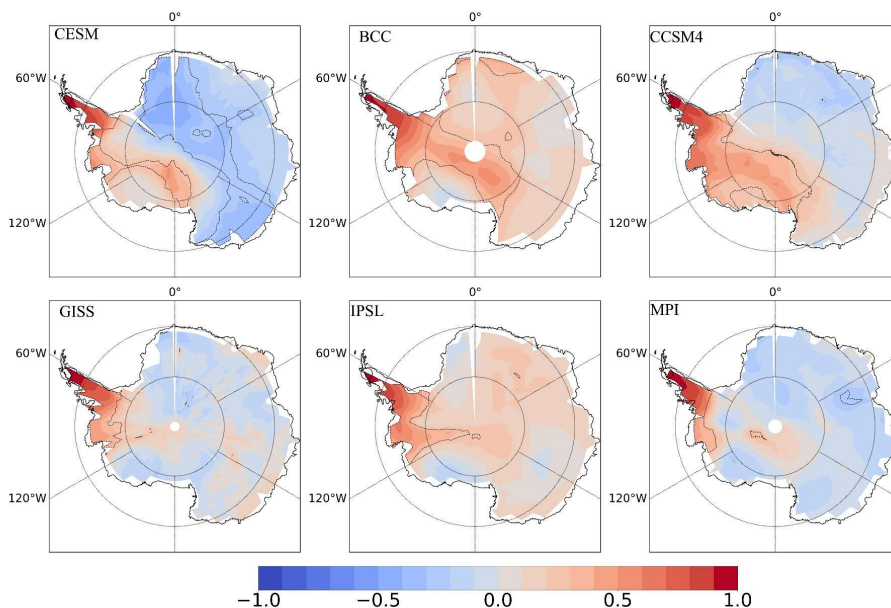
389 The second metric is the surface temperature trend over the period from 1825 C.E. to 1925 C.E. at Larissa, with the  
390 magnitude of  $-0.94 \pm 0.12$  °C/century. Fig. 8 shows the spatial correlation in the Antarctica Peninsula (AP). Despite  
391 the correlation coefficient decreasing as the grid getting far away from the Larissa, the values, at least around Larissa



392 for each model, are higher than 0.6, showing that this metric is representative of the whole peninsula region, and not  
393 extremely site-specific.

394 Figure 9 shows the same temperature trend (1825-1925) for all models. Overall, models are showing a warming  
395 trend (largest for CCSM, MPI and BCC), contradicting the observations, as highlighted already in Fig. 4c. A majority  
396 of the CESM members (CESM1, 7, 8, and 9) show a cooling trend over Antarctica, with CESM 1 and CESM 7 being  
397 able to capture the observed trend.

398 The 19th century is a time period when the Northern Hemisphere has started warming, whereas Southern  
399 Hemisphere records (Neukom et al., 2014), and specifically Antarctica, show no general warming trend (Stenni et al.,  
400 2017). Models tend to over-estimate the interhemispheric synchronicity (Neukom et al., 2014), and show a warming  
401 trend also in Antarctica, possibly in response to the anthropogenic forcing. This metric is thus an important tool for  
402 future research to evaluate whether the model data mismatch is due to internal variability (which will be investigated  
403 with more ensembles of the same model), or to an overestimated sensitivity to the anthropogenic forcing.



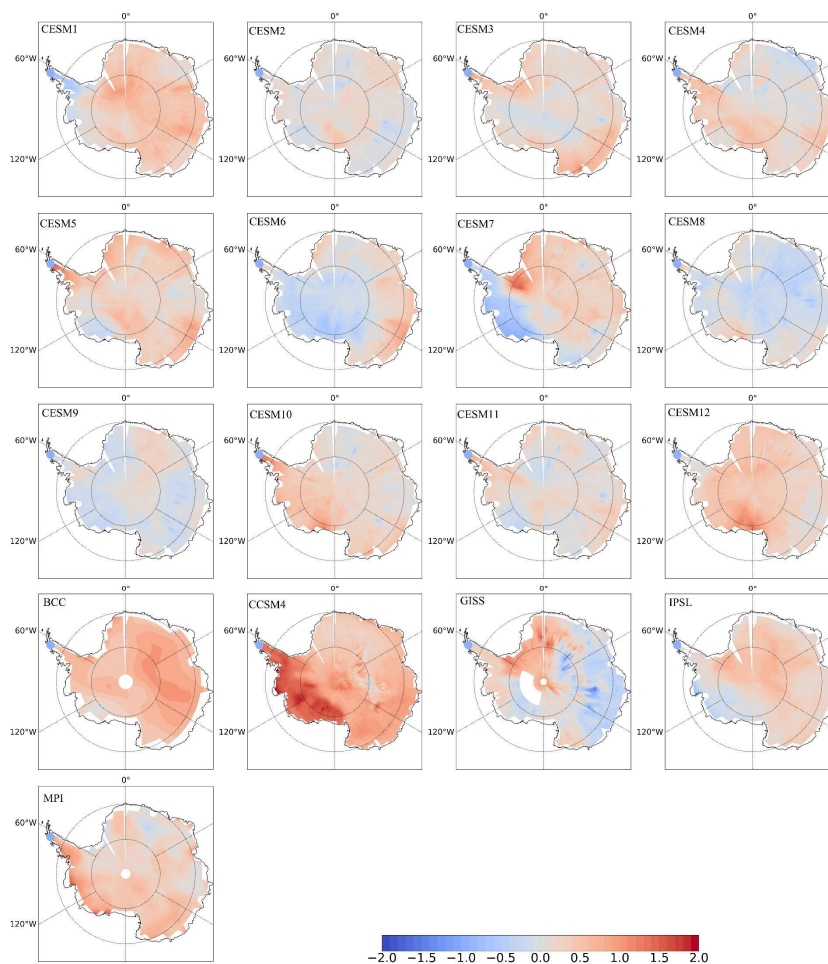
404

405 **Figure 8.** The correlation map (blue-red shading area) showing the relationship between the temperature from 1825 C.E. to 1925  
406 C.E. at Larissa and other grids in AP for each climate models. The black dotted contour lines show a significant correlation at the 99  
407 % significant level.

408



409



410

411 **Figure 9.** The simulated (blue-red shading area) and observed (circle) surface temperature trend from 1825 to 1925 C.E.

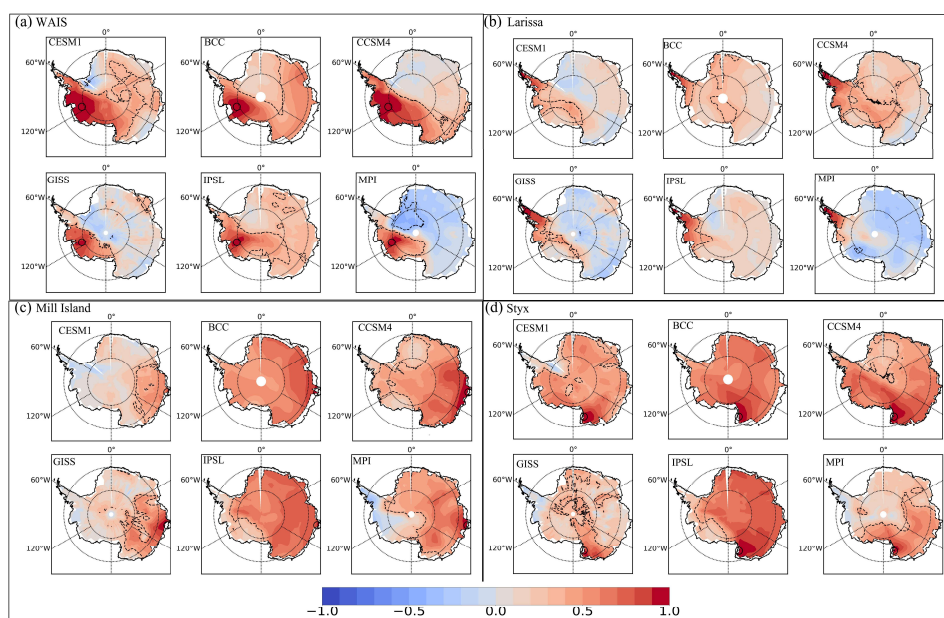
### 412 **4.3 Metric 3: recent warming trend**

413 The warming trend of the last 50 years is one of the clearest features of the observations. The intensification of the  
414 Southern Annular mode, in response to the Ozone hole is expected to produce a strong warming in the Antarctic  
415 Peninsula (incl. Larissa), and cooling on the Antarctic Coast (incl. Styx and Mill Island). WAIS has also been warming  
416 significantly over the past decades, and this trend is attributed to variability in the strength and position of the  
417 Amundsen Sea low pressure system (Jones et al., 2016). Here we propose a metric of the warming trend from 1950 to  
418 2005 at each of the four sites, to investigate whether model can reproduce these features.

419 First we look at the spatial correlation of the temperature between each site and other grid points (Fig. 10). The  
420 correlation is calculated on annual data for 1950 to 2005 C.E.. It is clear that each of our borehole temperature sites  
421 gives information about different sectors of Antarctica. Generally speaking, WAIS is representative of the



422 West-Antarctic continent, with a more pronounced dipole between WAIS and the Weddell sea section in MPI, and  
423 a lesser extent CESM and GISS. Larissa is representative of the Antarctic Peninsula as a whole, and from this  
424 resolution of climate model runs, there is no evidence of a dipole between either side of the Transantarctic mountains.  
425 Similar to WAIS, MPI has the strongest expression of a dipole between the Antarctic Peninsula and East Antarctica, a  
426 feature that is weaker but also present in GISS. A model that responds clearly to the Ozone forcing, and has a strong  
427 SAM signature should exhibit this dipole pattern, and it is interesting that some models do not show it, indicating that  
428 the Ozone forcing is not dominating over internal variability. Mill Island is generally representative of the Wilkes  
429 Land sector of East Antarctica, with the largest spatial homogeneity for BCC and IPSL (Fig. 10c). Finally, for Styx,  
430 the models with the largest spatial homogeneity (BCC and IPSL) show a strong correlation between Victoria Land and  
431 the rest of East Antarctica.



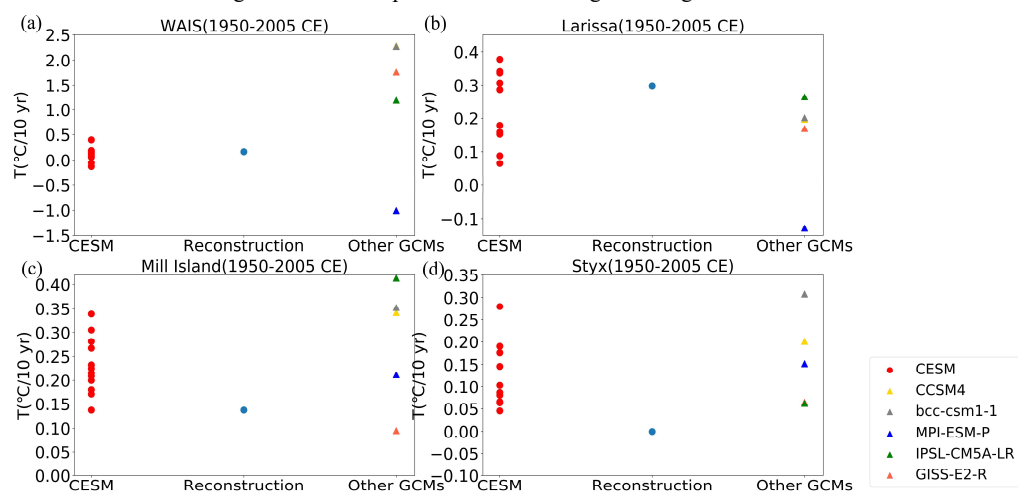
432  
433 **Figure 10.** The correlation map showing the relationship between the temperature from 1950 C.E. to 2005 C.E. at WAIS (a), Larissa  
434 (b), Mill Island (c), Styx (d) and other grids for each climate models. The red dashed contour lines show a significant correlation at  
435 the 99 % significant level.

436 Figure 11 shows the surface temperature trend from 1950 to 2005 C.E. The strong warming trend at Larissa is  
437 underestimated in most models (Fig. 11 (b)). MPI, which shows a clear dipole between the Peninsula and East  
438 Antarctica (Fig. 10) surprisingly does not show a warming trend at Larissa. This suggests that further work is needed  
439 to diagnose the changes in SAM in those models, and the response of SAM to ozone and greenhouse gas forcing.  
440 Additionally, three out of twelve CESM simulations indicate cooling in West Antarctica, which is coherent with the  
441 hypothesis that the observed warming is due to unforced variability and that models are not expected to match this  
442 trend perfectly. The warming at Mill Island is relatively well reproduced. However, none of the models can reproduce



443 the weak cooling seen at Styx. The lower spatial representivity of this site (Fig. 10) lead us to interpret this as local  
444 processes missing in low resolution GCMs, such as the correct topography to account for the katabatic wind forcing,  
445 rather than a general failure of models to represent reality.

446 To sum up, the 1950 to 2005 trend at Larissa of  $0.29^{\circ}\text{C}/10\text{-years}$  is a useful benchmark for climate models to test  
447 their response to the Ozone forcing and the temperature pattern associated with the SAM index and other modes of  
448 variability influencing the Peninsula. The trend at Mill Island of  $0.14^{\circ}\text{C}/10\text{-years}$  is a useful target to ensure that  
449 Antarctica is not warming too much in response to Greenhouse gas forcing.



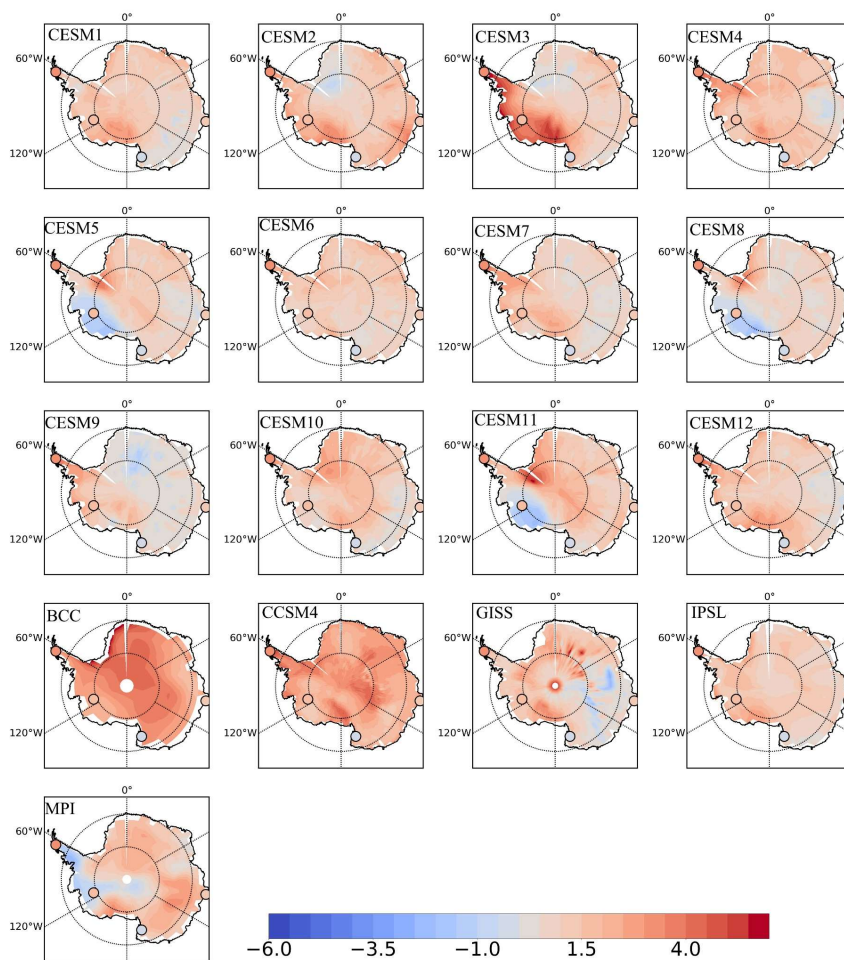
450

451 **Figure 11.** Linear trends for the four boreholes over 1950 to 2005 C.E.: (a) WAIS; (b) Larissa; (c) Mill Island; (d) Styx

452



453



454

455 **Figure 12.** The simulated (blue-red shading area) and observed (circle) surface temperature trend from 1950 to 2005 C.E  
456 Antarctica.

## 457 5. Conclusion

458 In this study, we test two complementary ways to evaluate the climate model performance using borehole temperature  
459 observations. The standard way is to compare the reconstruction of surface temperature with simulated values in the  
460 time domain. The successful application here of a forward model driven with climate model results provides an  
461 additional way to analyze jointly model results and borehole temperature measurements. Compared to the model-data  
462 comparison in the time domain, the forward model allows us to reproduce the subsurface temperature profiles and to  
463 compare them directly with measured borehole temperature profiles.



464 The comparison of the surface temperature time series is simpler and more straightforward but it is limited by the  
465 different resolutions of the reconstructions and climate model results. Nevertheless, some robust conclusions can be  
466 derived from this model-data comparison that are confirmed by the direct analyses of the temperature profiles as a  
467 function of the depth. For instance, the long-term cooling trend over last millennium observed at WAIS is relatively  
468 well reproduced in all models but with a weaker amplitude, which means the model maybe miss some feedbacks or  
469 low-frequency internal variability. Most simulations agree with data on a recent warming but the magnitude and  
470 timing vary a lot between models for the four sites. The large variability of the trends over the 20th century within the  
471 CESM ensemble for WAIS and Larissa suggests that many apparent model disagreements for those sites can be due to  
472 internal variability while the disagreement for Styx and Mill Island may be related to local processes not captured by  
473 global models.

474 The comparison of the model output and data in the depth domain is useful because the borehole temperature  
475 inversion is an under-determined problem, and many different temperature histories could fit the data equally well.  
476 The comparison of the temperature profiles confirms the conclusions found in the time domain, and validates the  
477 significance of some of the differences found. Some features are however difficult to interpret, such as the depth of the  
478 temperature minimum at the WAIS Divide site, which is not in the same order (deeper = older) as the timing of the  
479 temperature minimum between simulations. This points to the complexity of the interpretation of the borehole  
480 profiles, and the complementary use of the analyses in the depth and time domain.

481 Finally, some metrics derived from the corresponding reconstructions are proposed to be used more widely in model  
482 evaluation. The metrics used are demonstrated to be representative of a large spatial area, although they are calculated  
483 at a specific site. The results confirm that no models can reproduce the cooling during 19th over the AP and the weak  
484 warming over last 50-years in northern Victoria Land. Nevertheless, these models can capture the larger long-term  
485 cooling from 1000 to 1600 C.E. in West Antarctica, and the recent 50 years warming in West Antarctica and AP. This  
486 work brings quantitative tools to evaluate models and better simulate the Antarctic climate and its response to  
487 forcings.

488 *Data availability* The PMIP3/CMIP5 model results can be downloaded online from the Program for Climate Model  
489 Diagnosis and Intercomparison (PCMDI; <http://pcmdi9.llnl.gov>, last access: 20 April 2018). The Forward Model is  
490 available by request to Anais Orsi ([anais.orsi@lsce.ipsl.fr](mailto:anais.orsi@lsce.ipsl.fr)).

491 *Competing interests* The authors declare that there is no conflict of interest.

492 *Acknowledgements* We acknowledge the World Climate Research Programme Working Group on Coupled  
493 Modelling, which is responsible for CMIP, and we thank the climate modelling groups for producing and making  
494 available their model outputs. This work was supported by the by Chinese Government Scholarships (grant no.  
495 201806040211) and the Belgian Research Action through Interdisciplinary Networks (BRAIN-be) from Belgian  
496 Science Policy Office in the framework of the project "East Antarctic surface mass balance in the Anthropocene:  
497 observations and multiscale modelling (Mass2Ant)" (Contrat n° 15 BR/165/A2/Mass2Ant). Hugues Goosse is the  
498 research director within the F.R.S.-FNRS. A. Orsi was supported by the french national programme LEFE/INSU  
499 ABN2K.





## 500 References

- 501 Alley, R. B. and Koci, B. R.: Recent warming in central Greenland?, *Ann Glaciol*, 14(1977), 6–8,  
502 doi:<https://doi.org/10.3189/S0260305500008144>, 1990.
- 503 Abram N.J., H. V. McGregor, J. E. Tierney, M.N. Evans, N.P. McKay, D.S. Kaufman and the PAGES 2k Consortium,  
504 Early onset of industrial-era warming across the oceans and continents. *Nature*, 536, doi:  
505 <https://doi.org/10.1038/nature19082>, 411–418, 2016
- 506 Barrett, B. E., Nicholls, K. W., Murray, T., Smith, A. M. and Vaughan, D. G.: Rapid recent warming on Rutford Ice  
507 Stream, West Antarctica, from borehole thermometry, *Geophys Res Lett*, 36(2), 1–5, doi:10.1029/2008GL036369,  
508 2009.
- 509 Beltrami, H., Ferguson, G. and Harris, R. N.: Long-term tracking of climate change by underground temperatures,  
510 *Geophys Res Lett*, 32(19), 1–4, doi:10.1029/2005GL023714, 2005.
- 511 Beltrami, H., González-Rouco, J. F. and Stevens, M. B.: Subsurface temperatures during the last millennium: Model  
512 and observation, *Geophys Res Lett*, 33(9), 2–5, doi:10.1029/2006GL026050, 2006.
- 513 Bodri, Louise, and Vladimir Cermak. *Borehole climatology: a new method how to reconstruct climate*. Elsevier, 2011.
- 514 Braconnot, P., Harrison, S. P., Kageyama, M., Bartlein, P. J., Masson-Delmotte, V., Abe-Ouchi, A., Otto-Bliesner, B.  
515 and Zhao, Y.: Evaluation of climate models using palaeoclimatic data, *Nat Clim Chang*, 2(6), 417–424,  
516 doi:10.1038/nclimate1456, 2012
- 517 Chapman, W. L. and Walsh, J. E.: A synthesis of Antarctic temperatures, *J Clim*, 20(16), 4096–4117,  
518 doi:10.1175/JCLI4236.1, 2007.
- 519 Cuffey, K., and W. Paterson, *The Physics of Glaciers*, Academic, Amsterdam, 2010.
- 520 Dahl-Jensen, D., Morgan, V. I. and Elcheikh, A.: Monte Carlo inverse modelling of the Law Dome (Antarctica)  
521 temperature profile, *Ann Glaciol*, 29(1), 145–150, doi: <https://doi.org/10.3189/172756499781821102>, 1999.
- 522 Dee, S., Emile-Geay, J., Evans, M. N., Allam, A., Steig, E. J. and Thompson: PRYSM: An open-source framework for  
523 Proxy System Modeling, with applications to oxygen-isotope systems, *J Adv Model Earth Syst*, 6, 513–526,  
524 doi:10.1002/2013MS000282. Received, 2014.
- 525 Dufresne, J. L., Foujols, M., Denvil, S., Caubel, A., Marti, O., Aumont, O., Balkanski, Y., Bekki, S., Bellenger, H.,  
526 Benschila, R., Bony, S., Bopp, L., Braconnot, P., Brockmann, P., Cadule, P., Cheruy, F., Codron, F., Cozic, A.,  
527 Cugnet, D., de Noblet, N., Duvel, J. P., Ethé, C., Fairhead, L., Fichet, T., Flavoni, S., Friedlingstein, P., Grandpeix,  
528 J. Y., Guez, L., Guilyardi, E., Hauglustaine, D., Hourdin, F., Idelkadi, A., Ghattas, J., Jous- saume, S., Kageyama,  
529 M., Krinner, G., Labetoulle, S., Lahel- lec, A., Lefebvre, M. P., Lefevre, F., Levy, C., Li, Z. X., Lloyd, J., Lott, F.,  
530 Madec, G., Mancip, M., Marchand, M., Masson, S., Meurdesoif, Y., Mignot, J., Musat, I., Parouty, S., Polcher, J.,  
531 Rio, C., Schulz, M., Swingedouw, D., Szopa, S., Talandier, C., Terray, P., Viovy, N., and Vuichard, N.: Climate  
532 change projections us- ing the IPSL-CM5 Earth System Model: From CMIP3 to CMIP5, *Clim. Dyn.*, 40, 2123–  
533 2165, <https://doi.org/10.1007/s00382-012- 1636-1>, 2013.
- 534 Evans, M. N., Tolwinski-Ward, S. E., Thompson, D. M. and Anchukaitis, K. J.: Applications of proxy system  
535 modeling in high resolution paleoclimatology, *Quat Sci Rev*, 76, 16–28, doi:10.1016/j.quascirev. 2013.



- 536 García-García, A., Cuesta-Valero, F. J., Beltrami, H. and Smerdon, J. E.: Simulation of air and ground temperatures in  
537 PMIP3/CMIP5 last millennium simulations: Implications for climate reconstructions from borehole temperature  
538 profiles, *Environ Res Lett*, 11(4), doi:10.1088/1748-9326/11/4/044022, 2016.
- 539 Gent, P. R., Danabasoglu, G., Donner, L. J., Holland, M. M., Hunke, E. C., Jayne, S. R., Lawrence, D. M., Neale, R.  
540 B., Rasch, P. J., Vertenstein, M., Worley, P. H., Yang, Z.-L., and Zhang, M.: The Community Climate System  
541 Model Version 4, *J. Clim.*, 24, 4973–4991, <https://doi.org/10.1175/2011JCLI4083.1>, 2011.
- 542 González-Rouco, F., Von Storch, H. and Zorita, E.: Deep soil temperature as proxy for surface air-temperature in a  
543 coupled model simulation of the last thousand years, *Geophys Res Lett*, 30(21), 1–4, doi:10.1029/2003GL018264,  
544 2003.
- 545 González-Rouco, J. F., Beltrami, H., Zorita, E. and von Storch, H.: Simulation and inversion of borehole temperature  
546 profiles in surrogate climates: Spatial distribution and surface coupling, *Geophys Res Lett*, 33(1), 2–5,  
547 doi:10.1029/2005GL024693, 2006.
- 548 Goosse, H., Crowley, T.J., Zorita, E., Ammann, C.M., Renssen, H. and Driesschaert, E.: Modelling the climate of the  
549 last millennium: What causes the differences between simulations?. *Geophysical Research Letters*, 32(6), [https://](https://doi.org/10.1029/2005GL022368)  
550 doi.org/10.1029/2005GL022368, 2005.
- 551 Goosse, H., Braida, M., Crosta, X., Mairesse, A., Masson-Delmotte, V., Mathiot, P., Neukom, R., Oerter, H.,  
552 Philippon, G., Renssen, H., Stenni, B., van Ommen, T. and Verleyen, E.: Antarctic temperature changes during the  
553 last millennium: evaluation of simulations and reconstructions, *Quat Sci Rev*, 55, 75–90,  
554 doi:10.1016/j.quascirev.2012.09.003, 2012.
- 555 Harris, R. N. and Gosnold, W. D.: Comparisons of borehole temperature – depth profiles and surface air temperatures  
556 in the northern plains of the USA, *Geophys J Int*, 138(2), 541–548, doi: doi.org/10.1046/j.1365-246X. 1999.
- 557 Jones, J. M., Gille, S. T., Goosse, H., Abram, N. J., Canziani, P. O., Charman, D. J., Clem, K. R., Crosta, X., De  
558 Lavergne, C., Eisenman, I., England, M. H., Fogt, R. L., Frankcombe, L. M., Marshall, G. J., Masson-Delmotte, V.,  
559 Morrison, A. K., Orsi, A. J., Raphael, M. N., Renwick, J. A., Schneider, D. P., Simpkins, G. R., Steig, E. J., Stenni,  
560 B., Swingedouw, D. and Vance, T. R.: Assessing recent trends in high-latitude Southern Hemisphere surface  
561 climate, *Nat Clim Chang*, 6(10), 917–926, doi:10.1038/nclimate3103, 2016.
- 562 Klein, F., Goosse, H., Graham, N. E. and Verschuren, D.: Comparison of simulated and reconstructed variations in  
563 East African hydroclimate over the last millennium, *Clim Past*, 12(7), 1499–1518, doi:10.5194/cp-12-1499-2016,  
564 2016.
- 565 Klein, F., Abram, N. J., Curran, M. A. J., Goosse, H., Goursaud, S., Masson-delmotte, V., Moy, A., Neukom, R., Orsi,  
566 A., Sjolte, J., Steiger, N., Stenni, B. and Werner, M.: Assessing the robustness of Antarctic temperature  
567 reconstructions over the past two millennia , *Clim Past*, 661–684, doi: doi.org/10.5194/cp-15-661-2019, 2019.
- 568 Smith, K. L. and Polvani, L. M.: Spatial patterns of recent Antarctic surface temperature trends and the importance of  
569 natural variability: lessons from multiple reconstructions and the CMIP5 models, *Clim Dyn*, 48(7–8), 2653–2670,  
570 doi:10.1007/s00382-016-3230-4, 2017.



- 571 Ljungqvist, F. C., Zhang, Q., Brattström, G., Krusic, P. J., Seim, A., Li, Q., ... & Moberg, A.. Centennial-Scale  
572 Temperature Change in Last Millennium Simulations and Proxy-Based Reconstructions. *Journal of Climate*, 32(9),  
573 2441-2482. <https://doi.org/10.1175/JCLI-D-18-0525.1>, 2019.
- 574 Muto, A., Scambos, T. A., Steffen, K., Slater, A. G. and Clow, G. D.: Recent surface temperature trends in the interior  
575 of East Antarctica from borehole firn temperature measurements and geophysical inverse methods, *Geophys Res*  
576 *Lett*, 38(15), 6-11, doi: 10.1029/2011GL048086, 2011.
- 577 Nagornov, O. V., Konovalov, Y. V., Zagorodnov, V. S., & Thompson, L. G. Reconstruction of the surface  
578 temperature of Arctic glaciers from the data of temperature measurements in wells. *Journal of engineering physics*  
579 *and thermophysics*, 74(2), 253-265, doi: [doi.org/10.1023/A:101666161](https://doi.org/10.1023/A:101666161), 2001.
- 580 Nagornov, O. V., Konovalov, Y. V. and Tchijov, V.: Temperature reconstruction for Arctic glaciers, *Palaeogeogr*  
581 *Palaeoclimatol Palaeoecol*, 236(1-2), 125-134, doi: 10.1016/j.palaeo.2005.11.035, 2006.
- 582 Neukom, R., Gergis, J., Karoly, D. J., Wanner, H., Curran, M., Elbert, J., González-Rouco, F., Linsley, B. K., Moy, A.  
583 D., Mundo, I., Raible, C. C., Steig, E. J., Van Ommen, T., Vance, T., Villalba, R., Zinke, J. and Frank, D.:  
584 Inter-hemispheric temperature variability over the past millennium, *Nat Clim Chang*, 4(5), 362-367,  
585 doi:10.1038/nclimate2174, 2014.
- 586 Nicolas, J. P. and Bromwich, D. H.: New reconstruction of antarctic near-surface temperatures: Multidecadal trends  
587 and reliability of global reanalyses, *J Clim*, 27(21), 8070-8093, doi:10.1175/JCLI-D-13-00733.1, 2014.
- 588 Orsi, A. J., Cornuelle, B. D. and Severinghaus, J. P.: Little Ice Age cold interval in West Antarctica: Evidence from  
589 borehole temperature at the West Antarctic Ice Sheet (WAIS) Divide, *Geophys Res Lett*, 39(9), 1-7,  
590 doi:10.1029/2012GL051260, 2012.
- 591 Otto-Bliesner, B. L., Brady, E. C., Fasullo, J., Jahn, A., Landrum, L., Stevenson, S., Rosenbloom, N., Mai, A., and  
592 Strand, G.: Cli- mate variability and change since 850 C.E. An ensemble ap- proach with the Community Earth  
593 System Model (CESM), *B. Am. Meteor. Soc.*, 97, 735-754, <https://doi.org/10.1175/BAMS-D-14-00233.1>, 2016.
- 594 Rath, V., Rouco, J. F. G. and Goosse, H.: Impact of postglacial warming on borehole reconstructions of last  
595 millennium temperatures, *Clim Past*, 8(3), 1059-1066, doi:10.5194/cp-8-1059-2012, 2012.
- 596 Renssen, H., Goosse, H., Fichefeti, T., Masson-delmotte, V., Ko, N., Lemaftre, G., Louvain, D. and Cyclotron, C.:  
597 Holocene climate evolution in the high-latitude Southern Hemisphere simulated by a coupled atmosphere-sea  
598 ice-ocean-vegetation model, , 7, 951-964, 2005.
- 599 Roberts, J. L., Moy, A. D., Van Ommen, T. D., Curran, M. A. J., Worby, A. P., Goodwin, I. D. and Inoue, M.:  
600 Borehole temperatures reveal a changed energy budget at Mill Island, East Antarctica, over recent decades,  
601 *Cryosphere*, 7(1), 263-273, doi:10.5194/tc-7-263-2013, 2013.
- 602 Schmidt, G. A., Jungclaus, J. H., Ammann, C. M., Bard, E., Braconnot, P. C. T. J. D. G., Crowley, T. J., ... &  
603 Otto-Bliesner, B. L. Climate forcing reconstructions for use in PMIP simulations of the last millennium (v1. 0).  
604 *Geoscientific Model Development*, 4(1), 33-45, doi: 10.5194/gmd-4-33-2011, 2011.
- 605 Schmidt, G. A., Jungclaus, J. H., Ammann, C. M., Bard, E., Bra- connot, P., Crowley, T. J., Delaygue, G., Joos, F.,  
606 Krivova, N. A., Muscheler, R., Otto-Bliesner, B. L., Pongratz, J., Shindell, D. T., Solanki, S. K., Steinhilber, F., and



- 607 Vieira, L. E. A.: Cli-  
608 mate forcing reconstructions for use in PMIP simulations of the Last Millennium (v1.1),  
609 *Geosci. Model Dev.*, 5, 185–191, <https://doi.org/10.5194/gmd-5-185-2012>, 2012.
- 610 Schmidt, G. A., Kelley, M., Nazarenko, L., Ruedy, R., Russell, G. L., Aleinov, I., Bauer, M., Bauer, S. E., Bhat, M. K.,  
611 Bleck, R., Canuto, V., Chen, Y., Cheng, Y., Clune, T. L., Genio, A. D., Fainchtein, R. D., Faluvegi, G., Hansen, J. E.,  
612 Healy, R. J., Kiang, N. Y., Koch, D., Lacis, A., Legrande, A. N., Lerner, J., Lo, K. K., Matthews, E. E., Menon, S.,  
613 Miller, R. L., Oinas, V., Oloso, A. O., Perlwitz, J. P., Puma, M. J., Put-  
614 man, W. M., Rund, D., Romanou, A., Sato,  
615 M., Shindell, D. T., Sun, S., Syed, R. A., Tausnev, N., Tsigaridis, K., Unger, N., Voulgarakis, A., Yao, M.-S., and  
616 Zhang, J.: Configura-  
617 tion and assessment of the GISS ModelE2 contributions to the CMIP5 archive, *J. Advan. in*  
618 *Mode. Earth Syst.*, 6, 141–184, <https://doi.org/10.1002/2013MS000265>, 2014.
- 619 Schneider, D. P., Steig, E. J., Ommen, T. D. Van, Dixon, D. A., Mayewski, P. A., Jones, J. M. and Bitz, C. M.:  
620 Antarctic temperatures over the past two centuries from ice cores, , 33(July), 1–5, doi:10.1029/2006GL027057,  
621 2006.
- 622 Smith, K. L., & Polvani, L. M. (2017). Spatial patterns of recent Antarctic surface temperature trends and the  
623 importance of natural variability: lessons from multiple reconstructions and the CMIP5 models. *Climate dynamics*,  
624 48(7-8), 2653-2670. <https://doi.org/10.1007/s00382-016-3230-4>
- 625 Steig, E. J., Schneider, D. P., Rutherford, S. D., Mann, M. E., Comiso, J. C. and Shindell, D. T.: Warming of the  
626 Antarctic ice-sheet surface since the 1957 International Geophysical Year, *Nature*, 457(7228), 459–462,  
627 doi:10.1038/nature07669, 2009.
- 628 Stenni, B., Curran, M. A. J., Abram, N. J., Orsi, A., Goursaud, S., Masson-Delmotte, V., Neukom, R., Goosse, H.,  
629 Divine, D., Van Ommen, T., Steig, E. J., Dixon, D. A., Thomas, E. R., Bertler, N. A. N., Isaksson, E., Ekaykin, A.,  
630 Werner, M. and Frezzotti, M.: Antarctic climate variability on regional and continental scales over the last 2000  
631 years, *Clim Past*, 13(11), 1609–1634, doi:10.5194/cp-13-1609-2017, 2017.
- 632 Stevens, B., Giorgetta, M., Esch, M., Mauritsen, T., Crueger, T., Rast, S., Salzmann, M., Schmidt, H., Bader, J., Block,  
633 K., Brokopf, R., Fast, I., Kinne, S., Kornblueh, L., Lohmann, U., Pincus, R., Reichler, T., and Roeckner, E.: The  
634 atmospheric com-  
635 ponent of the MPI-M earth system model: ECHAM6, *J. Adv. Model. Earth Syst.*, 5, 1–27,  
636 <https://doi.org/10.1002/jame.20015>, 2013.
- 637 Stevens, M. B., Gonza, J. F. and Beltrami, H.: North American climate of the last millennium: Underground  
638 temperatures and model comparison, 113, 1–15, doi:10.1029/2006JF000705, 2008.
- 639 Taylor, K. E., Stouffer, R. J., and Meehl, G. A.: An overview of CMIP5 and the experiment design, *B. Am. Meteorol.*  
640 *Soc.*, 93, 485–498, doi:10.1175/BAMS-D-11-00094.1, 2012.
- 641 Turner, J., Colwell, S. R., Marshall, G. J., Lachlan-Cope, T. A., Carleton, A. M., Jones, P. D., Lagun, V., Reid, P. A.  
642 and Iagovkina, S.: Antarctic climate change during the last 50 years, *Int J Climatol*, 25(3), 279–294,  
643 doi:10.1002/joc.1130, 2005.
- 644 Wu, T., Song, L., Li, W., Wang, Z., Zhang, H., Xin, X., Zhang, Y., Zhang, L., Li, J., Wu, F., Liu, Y., Zhang, F., Shi,  
645 X., Chu, M., Zhang, J., Fang, Y., Wang, F., Lu, Y., Liu, X., Wei, M., Liu, Q., Zhou, W., Dong, M., Zhao, Q., Ji, J.,  
646 Li, L., and Zhou, M.: An overview of BCC climate system model development and application for climate change  
647 studies, *J. Met. Res.*, 28, 34–56, <https://doi.org/10.1007/s13351-014-3041-7>, 2014.



- 644 Yang, J. W., Han, Y., Orsi, A. J., Kim, S. J., Han, H., Ryu, Y., Jang, Y., Moon, J., Choi, T., Hur, S. Do and Ahn, J.:  
645 Surface Temperature in Twentieth Century at the Styx Glacier, Northern Victoria Land, Antarctica, From Borehole  
646 Thermometry, *Geophys Res Lett*, 45(18), 9834–9842, doi:10.1029/2018GL078770, 2018.
- 647 Zagorodnov, V., Nagornov, O., Scambos, T. A., Muto, A., Mosley-Thompson, E., Pettit, E. C. and Tyufin, S.:  
648 Borehole temperatures reveal details of 20 th century warming at Bruce Plateau, Antarctic Peninsula, Cryosphere,  
649 6(3), 675–686, doi:10.5194/tc-6-675-2012, 2012.